AlScN High Electron Mobility Transistors: Integrating High Piezoelectric, High K Dielectric, and Ferroelectric Functionality

Joseph Casamento¹ (Invited), Kazuki Nomoto², Thai-Son Nguyen¹, Hyunjea Lee², Chandrasekhar Savant¹, Lei Li², Austin Hickman², Takuya Maeda³, Yu-Tsun Shao⁴ Jimy Encomendero², Ved Gund², Timothy Vasen⁵, Shamima Afroz⁵, Daniel Hannan⁵, David A. Muller^{4,6}, Huili Grace Xing^{1,2,3}, and Debdeep Jena^{1,2,3}

- 1 Department of Materials Science and Engineering, Cornell University, Ithaca, NY 14853, USA,
- 2 School of Electrical and Computer Engineering, Cornell University, Ithaca, NY 14853, USA
- 3 Kavli Institute at Cornell for Nanoscale Science, Cornell University, Ithaca, NY 14853, USA
- 4 School of Applied and Engineering Physics, Cornell University, Ithaca, New York 14853, USA
- 5 Northrop Grumman Mission Systems Advanced Technology Laboratory, Linthicum, Maryland 21090, USA 6 Department of Physics, Cornell University, Ithaca, New York 14853,USA

Abstract—This paper presents an overview of the promising physical properties of the aluminum scandium nitride (AlScN) ternary alloy system and its integration in radiofrequency heterostructure high electron mobility transistors (RF HEMTs). Specifically, heterostructures with AlScN demonstrate enhanced piezoelectric response and enhanced relative dielectric permittivity, as well as ferroelectric behavior. These promising physical phenomena are manifested in HEMTs that show larger on current densities compared to aluminum gallium nitride (AlGaN) HEMTs and display ferroelectric behavior. An overlook on future improvements in thin film deposition and device fabrication is discussed to fully maximize the potential devices and integrated circuits incorporating AlScN.

Keywords—AIN, scandium, GaN, radiofrequency, monolithic microwave integrated circuits, high electron mobility transistor, piezoelectric, high-K dielectric, ferroelectric

I. INTRODUCTION

The combination of high speed and high voltage operation stemming from robust two-dimensional electron gases (2DEG) that result from heterojunction polarization discontinuities make AlGaN-GaN HEMTs leading contenders for efficient power electronics for 6G systems and beyond [1]. This sets up an excellent platform to incorporate novel materials and physical properties. AlScN has demonstrated excellent physical properties that aim to enhance the performance and expand the functionality of nitride HEMTs. These promising physical properties include enhanced piezoelectric response, an enhanced relative dielectric permittivity, and ferroelectric behavior [2-7]. In addition, adding scandium to AlN increases the in-plane lattice parameter, allowing lattice-matching to GaN [8] and strain-engineered heterostructures. These properties have led to the commercial adoption of AlScN in high-performance acoustic devices such as bulk acoustic wave (BAW) resonators [9,10] and its utilization in GaN based HEMTs [11-13]. For example, an enhanced piezoelectric response increases the

bandwidth and electromechanical coupling coefficient of acoustic filters. An enhanced piezoelectric response increases the 2DEG density in strained HEMTs. Despite the promising physical properties, epitaxial AlScN is still at a relatively early stage of development. Improvements in thin film deposition and device fabrication are needed to maximize the performance of AlScN HEMTs that demonstrate high on-current densities, and high-K dielectric and ferroelectric behavior when AlScN is incorporated as a barrier layer.

II. HETEROINTERFACES, ENHANCED PIEZOELECTRICITY

A. <u>AlScN-GaN Heterointerfaces</u>

AlScN thin films were grown by plasma assisted molecular beam epitaxy (MBE) on n type GaN bulk substrates. Initially, AlScN was projected to be lattice-matched to GaN at between 12 and 18 % Sc from first principles calculations [14], similar to indium aluminum nitride (InAlN), so the reduced dislocation density from bulk substrates was expected to be advantageous to study fundamental growth trends. Nitrogen rich growth conditions (e.g., III/V ratio less than 1) were utilized to ensure Sc incorporation in the crystal and to mitigate the presence of undesired conductive Sc-Al intermetallic phases. To assess the structural quality of the AlScN-GaN interfaces and the crystallographic polarity across the heterojunction, high-angle annular dark field scanning transmission electron microscopy (HAADF-STEM) and accompanying annular bright field (ABF) imaging was utilized. Figure 1 illustrates the atomically abrupt nature of the AlScN (18 % Sc)-GaN interface. This is attributed to the removal of excess Ga before the AlScN growth and a AlScN growth temperature (e.g., 600C) that is compatible and/or the same as the existing GaN growth temperature. The epitaxial AlScN layer is seen to be metal polar, adopting the same polarity as the underlying GaN layer and substrate.

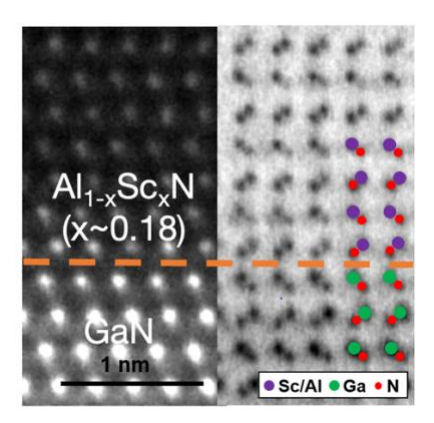


Figure 1: Combined HAADF and ABF STEM image of AlScN (18 % Sc)-GaN interface. In ABF, the nitrogen atoms are visible and denote metal polar orientations in each layer and across the interface. (From [3])

B. AlScN Enhanced Piezoelectricity

Significantly enhanced piezoelectric response discovered in 2009 in sputter deposited AlScN [2]. Specifically, an over 400% increase in the d₃₃ piezoelectric coefficient relative to AlN was achieved for Sc contents near 40 %. This led to the immense technological interest in acoustic technologies as AlN was the material of choice for acoustic filters in cellular phones. The electromechanical coupling coefficient, utilized as a figure of merit that is related to material properties such as stiffness and piezoelectric response, depends on the degree of caxis orientation of the crystal. To push acoustic filters to higher operating frequencies, developing a high degree of c-axis texture and a robust piezoelectric response at ultra-low thicknesses (e.g., under 100 nm) is needed. Figure 2 illustrates extracted d₃₃ piezoelectric coefficients from piezoresponse force microscopy (PFM), a scanning probe technique. The measured piezoelectric response increases up until ~ 18 % Sc, and decreases thereafter.

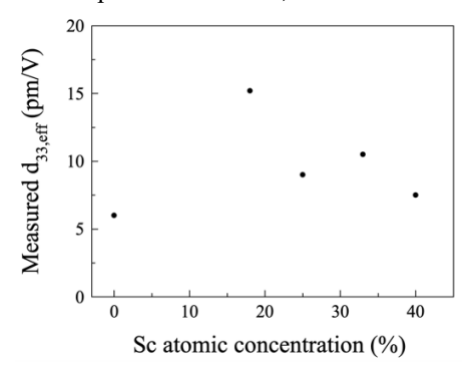


Figure 2: Measured d_{33,eff} piezoelectric coefficient from vertical piezoresponse force microscopy (PFM) of AlScN from 0 to 40 % Sc. (From [3])

C. AlScN Phase Inhomogeneity at high Sc Contents

Alloying Sc to AlN is shown to increase the in-plane lattice parameter and cause non-monotonic changes in the out-of plane lattice parameter [5,8]. This causes changes in critical thickness of these layers when grown on AlN and GaN. In addition, phase separation is predicted to be thermodynamically stable at high Sc contents due to the difference in crystal structures between ScN and AlN. ScN is stable in the face centered cubic crystal

This work was supported by the DARPA Tunable Ferroelectric Nitrides (TUFEN) program, the Semiconductor Research Corporation (SRC), and Northrop Grumman.

structure that is analogous to rocksalt (NaCl), which is non polar and non-centrosymmetric, and therefore does not display piezoelectric or spontaneous polarization. Accordingly, this is of high importance for technological applications as the piezoelectric enhancement occurs at larger Sc contents. Kinetic factors that arise during growth, in addition to layer thickness, affect the presence of phase inclusions. At 40 % Sc content, cubic zinc blende (not rocksalt) inclusions are observed, as shown in Figure 3. These inclusions are linked to partial dislocations around stacking faults. Controlling the presence of stacking faults in AlScN will be essential toward achieving phase pure AlScN at higher Sc contents.

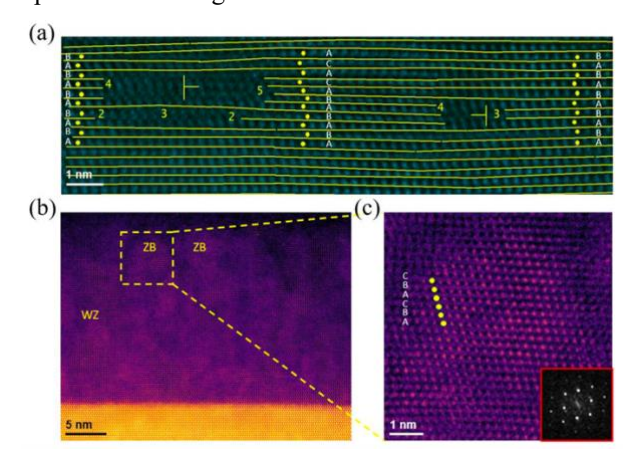


Figure 3: Stacking faults in AlScN (18, 40 % Sc). (a) Magnified region in the AlScN (18% Sc) film where wurtzite AB sequence stacking is observed and labeled. ABCB stacking is observed on the right side of the image, indicating a stacking fault. The numbers denoted on either side of the stacking fault indicate the number of planes, showing that the defects are partial dislocations associated with a stacking fault. (b) Low magnification image of the AlScN (40 % Sc) film grown on GaN, showing mainly wurtzite structure with zinc blende inclusions toward the surface of the film. (c) Magnified image from the yellow box from (b), showing the lattice ABC stacking. The diffractogram in the image inset confirms the zinc blende structure. (From [3])

III. HETEROINTERFACES, HIGH-K DIELECTRIC BEHAVIOR

A. AlScN High K Dielectric Origins, Dielectric Properties

Increased piezoelectric response in AlScN is a result of more compliant bonds, which stem from the more ionic bonding character introduced by substituting Al atoms with Sc. The larger degree of bond ionicity is also linked to enhanced polarizability in the valence electrons. This gives rise to a large atomic displacement and polarization change. For these reasons, a higher relative dielectric permittivity (ϵ_r) is expected when Sc is added to AlN. These expectations were corroborated with first principles calculations [5], which calculated an average out-of plane dielectric permittivity of ~ 15 for ~ 17 % Sc.

The dielectric properties of AlScN-n⁺GaN heterostructures were evaluated by capacitance-voltage measurements performed at room temperature and from 1 KHz to 10 MHz frequency, as shown in figure 4. The capacitance is relatively constant as a function of frequency, especially past 1 MHz frequency. This is indicative of ionic and electronic contributions to the relative dielectric permittivity, which are

expected to exist past 100 GHz frequencies. Measurement of the dielectric behavior at higher frequencies is of high interest for 6G applications and beyond.

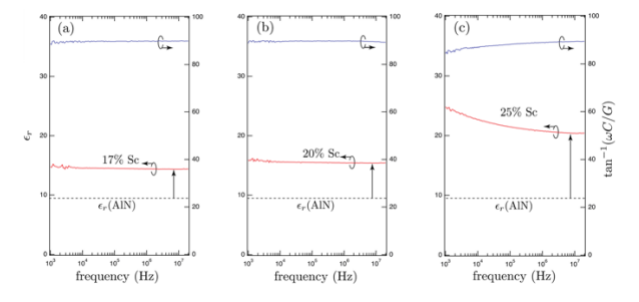


Figure 4: (a)–(c) Extracted relative dielectric permittivity (ε_r) at multiple measurement frequencies. The dispersion seen at low frequencies for 25% Sc is attributed to space charge polarization. (From [5])

Figure 5 shows a comparison between the low frequency relative dielectric permittivity of AlScN and common IIInitride semiconductors and dielectrics used for III-nitride electronic and photonic devices. AlScN (25 % Sc) has a value that is the highest of any existing III-nitride material ($\varepsilon_r \sim 21$) and comparable with other commonly utilized dielectrics such as HfO₂ and Ta₂O₅. It is important to note that although the ε_r value for InN is 15, the relatively low bandgap and conductive nature of InN has precluded its use as a dielectric material; and that AlScN does not suffer from these drawbacks. Since optical absorption measurements for bandgaps could not be performed directly on the AlScN-GaN heterostructures due to the smaller bandgap of GaN (3.4 eV), films of AlScN (0-25 % Sc) of 200 nm thicknesses were separately grown on AlN on c-plane sapphire substrates with the same growth conditions (e.g., III/V ratio, temperature) as those grown on n⁺ GaN discussed earlier. They show near optical absorption edges ranging from 6.0 to 5.1 eV (not shown).

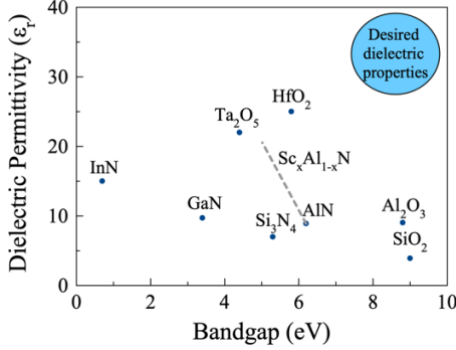


Figure 5: Comparison of low frequency relative dielectric permittivity and optical bandgap of common III-nitride semiconductors and dielectric materials utilized for III-nitride materials. The results for various Sc mole fraction AlScN discussed here are indicated along the dashed line. The AlScN bandgap values used are from separate AlScN samples grown on AlN on c-plane sapphire templates. (From [5])

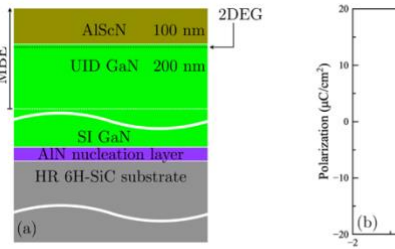
With a relatively large bandgap and relative dielectric permittivity, AlScN positions itself well for use as a dielectric

material for nitride HEMTs. A well-known hi-K metric for high-K oxides is the "equivalent oxide thickness" or EOT, which is defined relative to the SiO_2 dielectric thickness that has a low frequency ε_r of 3.9. Namely, a higher relative dielectric permittivity oxide material has a lower equivalent oxide thickness and is, therefore, attractive for vertical scaling of transistors. Here, the term can be extended to hi-K nitride dielectrics like AlScN for nitride HEMTs as an "equivalent nitride thickness" with a comparison to a Si_3N_4 dielectric thickness with a low frequency ε_r of 7.5 or Al(Ga)N. The ability to have an *in situ* high-K dielectric barrier layer is advantageous toward increasing the breakdown voltage and improving gain at higher frequencies in nitride HEMTs toward 6G applications.

IV. FERROELECTRIC HEMTS

A. AlScN Ferroelectric Origins, 2DEG as an Electrode

Enhanced piezoelectric and dielectric responses are prerequisites for ferroelectricity in oxide material systems. AlScN already having shown enhanced piezoelectric and dielectric behavior, was expected to be ferroelectric. In 2019, sputtered AlScN was shown to be ferroelectric [6]. For incorporation in nitride HEMTs and various devices outside of capacitors, the AlScN layer needs to be deposited in a way that maintains the 2DEG after growth and can utilize the 2DEG as a bottom electrode. Due to the ultra-wide bandgap of AlScN and type-I band offset, a 2DEG forms at the AlScN-GaN interface. The ferroelectric properties of a 100 nm thick AlScN - undoped GaN heterostructure are shown below in Figure 7. The 2DEG serves as the bottom electrode in this heterostructure and provides a pathway toward integrating novel functionality in ultra-thin AlScN layers.



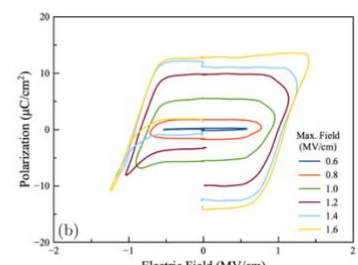


Figure 6: (a) Epitaxial AlScN/GaN heterostructure with unintentionally doped (UID) GaN, indicating a polarization-induced 2DEG at the heterojunction. (b) Measured P – E loops on diodes with Ti top electrode and the 2DEG of (a) as the bottom electrode, indicating ferroelectric behavior. (From [7])

B. <u>AlScN FerroHEMTs with Large On-Current Densities</u>

The enhanced piezoelectric polarization of the AlScN barrier layer enhances the electron density of the 2DEG prior to a critical thickness which saturates the 2DEG density. AlScN ferroelectric barrier layer HEMTs are expected to have large oncurrent densities and counterclockwise hysteresis in the drain current – gate voltage data. For simultaneous RF operation, an ultrathin AlScN barrier layer with a 90 nm length Ni T-gate is utilized. A schematic of the device is shown in Figure 8. Before

processing, room temperature van Der Pauw Hall effect measurements yielded a 2DEG with a sheet carrier concentration of $\sim 3 \times 10^{13} / \text{cm}^2$ and an electron mobility of ~ 456 cm²/Vs, resulting in a sheet resistance of ~ 450 Ω/sq .

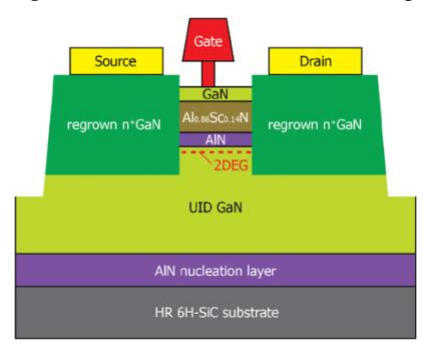


Figure 7: (a) Epitaxial AlScN/GaN heterostructure with a GaN cap, an AlScN barrier layer and an AlN interlayer. Regrown n⁺GaN serves as ohmic contacts to 2DEG, and a Ni T-gate is offset toward the source. (From [7])

The large on-current densities in excess of 4 A/mm in scaled devices are seen in the transfer characteristics plotted in Figure 8. The on-resistance is $\sim\!\!0.77~\Omega$ mm and the channel pinch off is a function of gate voltage. Large on-current densities are scalable with channel length as shown in Figure 9. The on-current densities for a 1 μm source-drain distance (L_{sd}) are among the largest among all reported semiconductor heterostructures.

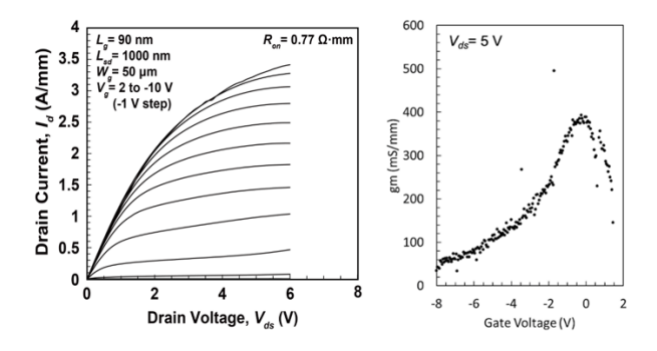


Figure 8: Transfer characteristics and transconductance (g_m) of AlScN FerroHEMTs with a peak g_m value of 0.4 S/mm.

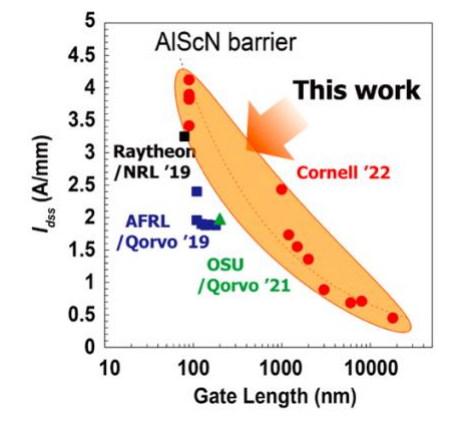


Figure 9: Scaling of on current with gate length in AlScN FerroHEMTs. (From [7])

Counterclockwise hysteresis is shown in Figure 10 with a memory window between 1.5 to 2 V. The subthreshold slope values range between 20-50 mV/decade at room temperature, indicating ferroelectric behavior of the AlScN layer. Future work will involve the study of various AlScN barrier layer thickness and device geometries to understand the interplay between charge trapping and ferroelectricity in these heterostructures.

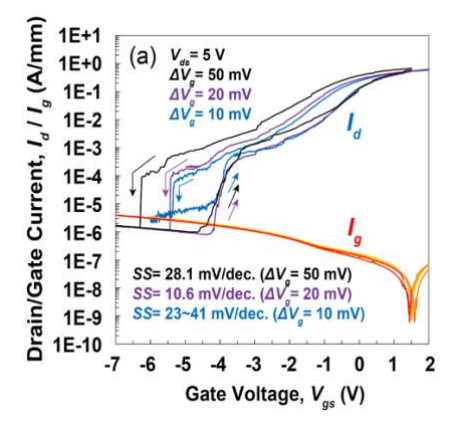


Figure 10: Scaling of output current with gate length in AlScN FerroHEMTs. (From [7])

C. AlScN FerroHEMT RF Performance

RF performance of the T-gate devices was measured from 50 MHz to 50 GHz. The measurements are calibrated using short, open, load, and through impedance standards on an alumina substrate. The extrapolation of both $|H_{21}|^2$ and U with -20 dB/dec slope gives the current gain cutoff frequency/maximum oscillation frequency f_T / f_{MAX} of 78/156 GHz after de-embedding, as shown in Figure 11. Further improvements in RF performance are expected with improvements in the contact resistance and utilization of surface passivation. Future work will also involve a detailed study of the parasitic capacitances in the heterostructures and their effects on f_T / f_{MAX} values.

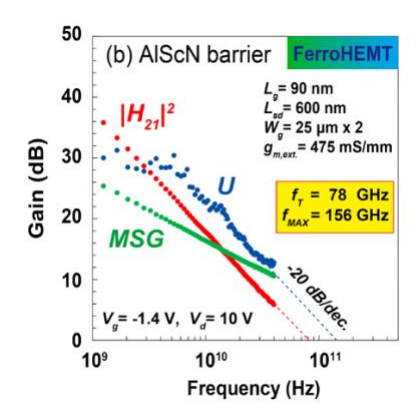


Figure 11: Measured cutoff frequencies of the AlScN barrier FerroHEMT with a 90 nm gate length ($L_{\rm g}$) and 600 nm $L_{\rm sd}$ (From [7])

D. AlScN-GaN Mutlichannel Heterostructures

The promising physical properties of AlScN have led to its adaptation in single channel devices. With the ability to lattice match to GaN, multichannel devices consisting of side gated and strain tunable AlScN-GaN heterostructures, for example, the superlattice castellated field effect transistors (SLCFETs) are a promising area of future work. Currently, AlGaN-GaN SLCFETs boast 4.8 A/mm on-current densities and over 10.8 W/mm output powers with 43 % power added efficiencies (PAE) at 94 GHz [15]. With a larger polarization discontinuity with GaN, AlScN based multichannel devices are expected to deliver larger on-currents and higher power densities at W band. Figure 12 shows a schematic of a AlScN-GaN multichannel heterostructure. Corresponding hall effect measurements at room temperature yield a total sheet carrier concentration of ~ 1×10^{14} /cm² and electron mobility of ~583 cm²/Vs. This leads to a low sheet resistance of $\sim 103 \ \Omega/\text{sq.}$, which is competitive with existing AlGaN-GaN multichannel devices [16].

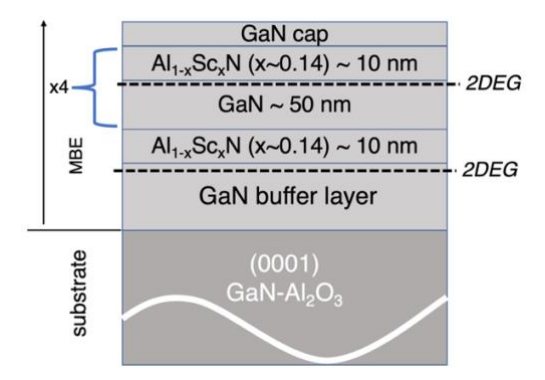


Figure 12: AlScN-GaN multilayer heterostructure with 5 channels. The GaN cap layer protects the underlying AlScN layer from oxidation.

V. CONCLUSIONS

In summary, promising electronic properties of AlScN including enhanced piezoelectric and dielectric response, in addition to ferroelectric behavior, are observed in epitaxial AlScN-GaN heterostructures. Scaled devices incorporating ultra-thin AlScN barrier layers and T-gates demonstrate high oncurrents and counterclockwise hysteresis in the output characteristics, illustrating ferroelectric behavior. These results are of high importance for energy efficient microelectronic and microphotonic systems for 6G applications and beyond. With improvements in material deposition and device fabrication, as well as engineered passivation layers and recess etching, RF performance will improve. In addition, novel functionalities such as reconfigurable E-D mode devices are expected.

ACKNOWLEDGMENT

This work was supported by Northrop Grumman Mission Systems university research funding. The authors would like to acknowledge the support from the DARPA

Tunable Ferroelectric Nitrides (TUFEN) program, monitored by Dr. Ronald Polcawich and Dr. Ali Keshavarzi. The authors would like to thank Ames Laboratory, DOE for supplying the Sc source material. This work was performed in part at the Cornell NanoScale Facility, a member of the National Nanotechnology Coordinated Infrastructure (NNCI), which is supported by the National Science Foundation (Grant NNCI-2025233). This work was performed in part at the Cornell NanoScale Facility, a member of the National Nanotechnology Coordinated Infrastructure (NNCI), which is supported by the National Science Foundation (Grant NNCI-2025233). The authors acknowledge the use of facilities and instrumentation supported by NSF through the Cornell University Materials Research Science and Engineering Center DMR-1719875.

REFERENCES

- [1] Patrick Fay, Debdeep Jena, and Paul Maki, GaN High Frequency Electronic Devices: Springer, 2019.
- [2] M. Akiyama et al, Adv. Mat., vol. 21, no. 5, p. 593, 2009.
- [3] J. Casamento et al, Appl. Phys. Lett., vol. 17, no. 11, p. 112101, 2020.
- [4] O. Ambacher et al, J. Appl. Phys., vol. 130, no. 4, p. 045102, 2021
- [5] J. Casamento et al, Appl. Phys. Lett., vol. 120, no. 15, p. 152901, 2022.
- [6] S. Ficthner, N. Wolff, F. Lofink, L. Kienle, and B. Wagner, J. Appl. Phys., vol. 125, no. 11, p. 114103, 2019.
- [7] J. Casamento et al, "FerroHEMTs: High-Current and High-Speed All Epitaxial AlScN/GaN Ferroelectric Transistors", International Electron Devices Meeting (IEDM), December 2022.
- [8] D.V. Dinh, J. Lahnemann, L. Geelhaar, and O. Brandt, Appl. Phys. Lett., vol. 122, no. 15, p. 152103, 2023
- [9] R. Vetury, A.S. Kochlar, and J.B. Shealy, "XBAW, An Enabling Technology for Next Generation Resonators and Filter Solutions for 5G and Wi-Fi 6/6E/7 applications", International Electron Devices Meeting (IEDM), December 2022.
- [10] Y. Zhang et al, "3D Monolithic Integration of ScAlN based GHz MEMS Acoustic Filters on 200mm RFSOI Wafer", International Electron Devices Meeting (IEDM), December 2022.
- [11] A.J. Green et al, IEEE Electron Device letters (EDL), vol. 40, no. 7, p. 1056, 2019.
- [12] E.M Chumbes et al, "ScAlN-GaN Transistor Technology for Millimeter-wave Ultra-high Power and Efficient MMICs," IEEE/MTT-S International Microwave Symposium – IMS, June 2022.
- [13] S. Krause et al, IEEE Electron Device letters (EDL), vol. 44, no. 1, p. 17, 2023.
- [14] M.A. Moram et al. J. Mater. Chem. A, vol. 15, no. 2, p. 6042,
- [15] R. S. Howell et al. "GaN SLCFET Technology for Next Generation mmW Systems, Demonstrating Pout of 10.87 W/mm With 43% PAE at 94 GHz," in *IEEE Microwave and Wireless Technology Letters*, vol. 33, no. 6, pp. 839-842, June 2023.
- [16] J.S Chang et al. "Advances in the Super-Lattice Castellated Field Effect Transistor (SLCFET) for High Power Density, Energy Efficient RF Amplification," in *IEEE MTT-S International Microwave Symposium (IMS)*, pp. 576-579, (2020) doi: 10.1109/IMS30576.2020